June 1987 LRP 324/87

Contributed Papers presented at the

14th European Conference on Controlled Fusion and Plasma Physics
Madrid, Spain - June 22-26, 1987

by the
TCA Team

STUDY OF THE PLASMA DYNAMIC RESPONSE TO ALFVEN WAVE HEATING POWER MODULATION IN TCA

B. Joye, J.B. Lister, J.-M. Moret

Centre de Recherche en Physique des Plasmas
Association Euratom - Confédération Suisse
Ecole Polytechnique Fédérale de Lausanne
21, avenue des Bains
CH-1007 LAUSANNE (Switzerland)

Studies of the dynamic response of the plasma to a modulated Alfvén Wave Heating (AWH) power have been performed on TCA. Radial analysis of the Soft-X ray flux modulation exhibits features similar to that of the sawtooth activity. Inside the q=1 surface, a constant phase shift is observed, while outside this radius the delay becomes important. The Alfvén Wave resonance layer structure has not yet been demonstrated to influence the phase profile. The power modulation has a strong effect on both the period and the crash amplitude of the sawteeth.

I. Introduction RF power modulation experiments on TCA were started [1] in an attempt to reveal features of the power deposition and heat transport profiles, an approach already used in ECRH experiments [2,3]. The present study concentrates on the Soft-X ray response, due to the reasonable radial resolution of the detector array and the influence of the electron temperature and the sawtooth activity on the signal. The AWH power and spectrum have already been shown to modify the sawtooth parameters [4]. The characteristics of the Soft-X ray response and the influence of the plasma current and of the Alfvén Wave spectrum will be presented in section III and IV, while sawtooth specific effects are described in section V.

II. Experimental conditions TCA plasmas (a=0.18m, R_o=0.61m, B_φ=1.52T) are heated by Alfvén Waves at 2.5MHz launched by an 8 group antenna system. A 50ms heating pulse is applied during the plasma current plateau; the power is modulated at a frequency between 100 and 500Hz with a mean continuous component up to 100kW and a depth of modulation up to 100%. The time constant associated with the modulation is of the order of or shorter than the global energy confinement time. In principle this should give rise to an easily measurable phase shift.
During the RF pulse the density increases and therefore the spectral conditions are scanned. To quantify the effects of the power modulation as the conditions vary, any given signal x(t') is fitted to the form : $x(t')=Re(\mathbf{X}(t))\cos(\omega t')+Im(\mathbf{X}(t))\sin(\omega t')+D(t)(t'-t)+\langle X\rangle(t)$, where $\mathbf{X}(t)$ is the complex amplitude of the modulated component. Both a significant drift and an offset are accounted for by the terms D(t)(t'-t) and $\langle X\rangle(t)$. The fit is carried out between t'-t=-5ms and t'-t=+5ms to obtain an adequate signal to noise ratio, giving a 10ms time resolution.
The Soft-X ray flux A(t) is measured by a 15-channel diode array with an 18mm spatial resolution. The dynamic response A* is estimated by the complex ratio $A^*=(A/\langle A\rangle)/P_{rf}$.

III. Effects on the Soft-X rays - the influence of the plasma current The profile of the amplitude |A*| and the phase of A* for a 126kA discharge are shown in Fig.1. The

density variation is small enough to guarantee that A is due to a modulation of the electron temperature for r<0.75a, but it could explain the fall of the phase in the outermost channels.

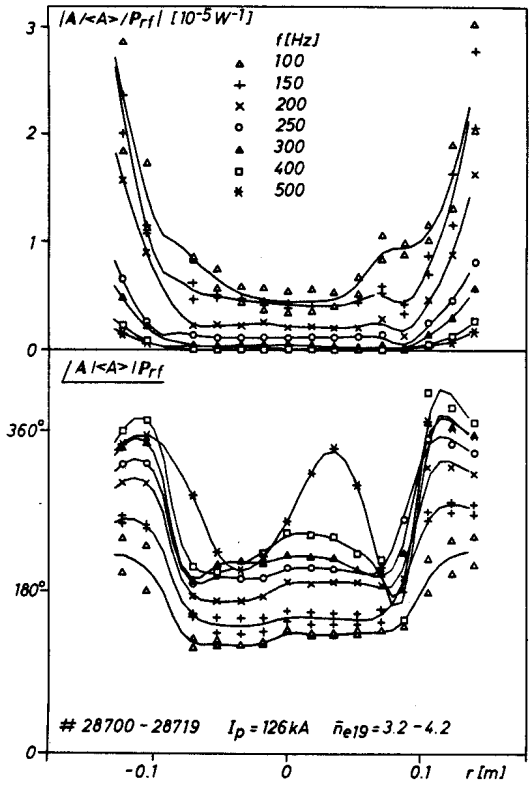

←Fig. 1 *Profile of the Soft-X ray response for different frequencies.*

↓Fig. 2 *Spectra of the Soft-X ray signal response for the central diode and for an outer diode.*

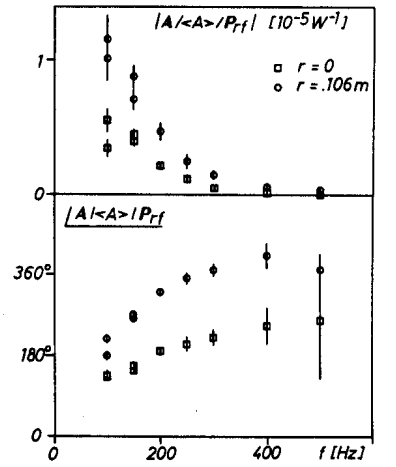

The spectra of the response of the central chord signal and of an outer channel signal, Fig. 2, both display the expected $1/\omega$ dependence of the amplitude but do not display the usual 90° phase shift expected in any directly heated region. The raw Soft-X ray signal of Fig.6 shows that both the base signal and the sawtooth parameters are modulated. The base line modulation, signature of a direct heating, is dominant only at low frequency when the central phase shift tends to 90°. The contribution of the modulation of the sawtooth characterisitics (Sect. IV) to **A*** explains the similarity between the **A*** and $\Delta A_{ST}/\langle A\rangle$ profiles.

In order to test the influence of the q=1 surface, results of a plasma current scan are shown in Fig.3. There is evidently a strong relation between the inversion radius and the **A*** profile shape (illustrated by the radius where the phase is 270° ($r_{270°}$ in the figure)). This scan confirms that the current profile plays a significant role in the plasma response to heating power.

IV. Effects on the Soft-X rays - the influence of the Alfvén Wave spectrum

During the density rise induced by the RF, the resonance layers already excited in the plasma are shifted outwards and new ones with different wave numbers appear in the centre [5]. To test whether the positions of these layers have an influence on the **A*** profiles, the temporal

evolution of $r_{270°}$ is plotted in Fig.4 for a 126kA discharge. Although the line average density rises from 2.5 to 5 x $10^{19}m^{-3}$, pushing the (n,m)=(2,0) surface out to r ≅ 0.75a, there is no visible influence on the phase profile. This is also shown in Fig.5 for which the toroidal excitation number N was changed. The shape of the phase profile is not altered although the change in N considerably modifies the resonance layer structure.

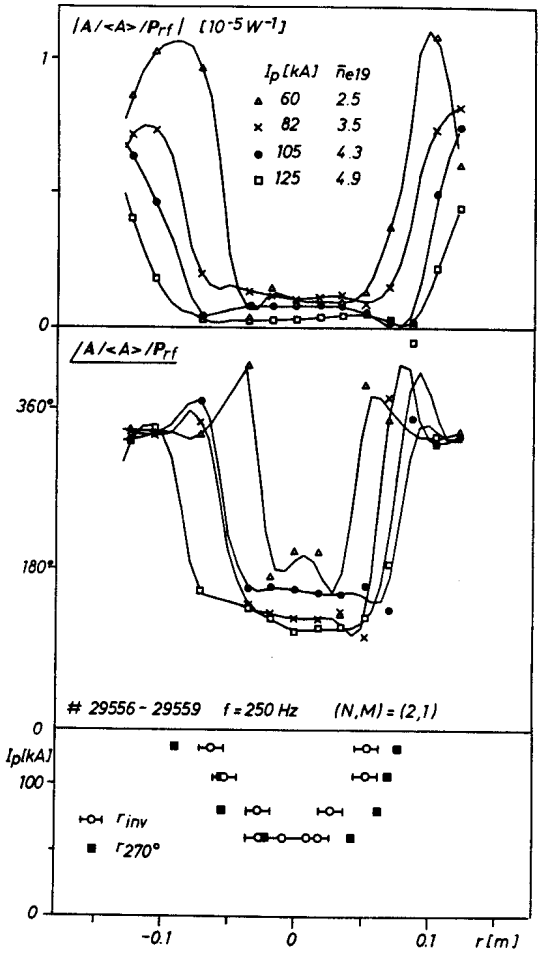

←Fig. 3 *Profile of the Soft-X ray response for different plasma currents.*

↓Fig. 4 *Time evolution of the radius where the phase is 270∞ together with the estimated position of resonance layers.*

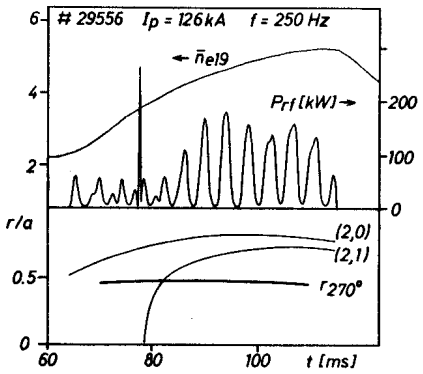

V. <u>Effects on the sawteeth</u> Fig.6 summarises the effect of the modulation on the sawtooth parameters. The relative amplitude of the crash on axis, $\Delta A_{ST}/<A>$, and the sawtooth period, ΔT_{ST}, are considerably affected. These both effects lead to a substantial effect on the amplitude and phase of the response A*. Surprisingly, the sawtooth slope $(\Delta A_{ST}/<A>)/\Delta T_{ST}$, which is roughly proportionnal to $dW_e(0)/dt$, is not in phase with P_{rf}. In fact the dominant influence of the RF lies in a modification of the sawtooth period. On the P_{rf} trace, where each cross represents a sawtooth crash, we see that 60% of them occur during the P_{rf} rise. This statistical result disappears at higher frequency. This observation suggests that the reaction of the sawtooth mechanism to the RF is not strictly related to a central energy deposition. Similar results were found in ICRH modulation experiments on JET [6] using a square wave modulation with a period much shorter than the sawtooth period.

VI. Conclusion RF modulation experiments on TCA clearly show that the dynamic response of the plasma to the RF power is dominated by sawtooth mechanisms. This forces us to take the sawtooth activity into account when interpreting the results in term of power deposition and heat diffusion. The plasma response is strongly related to the current profile, and this may possibly indicate a link with profile consistency. This provides a powerful tool to study the sawtooth influence in a RF heated Tokamak.

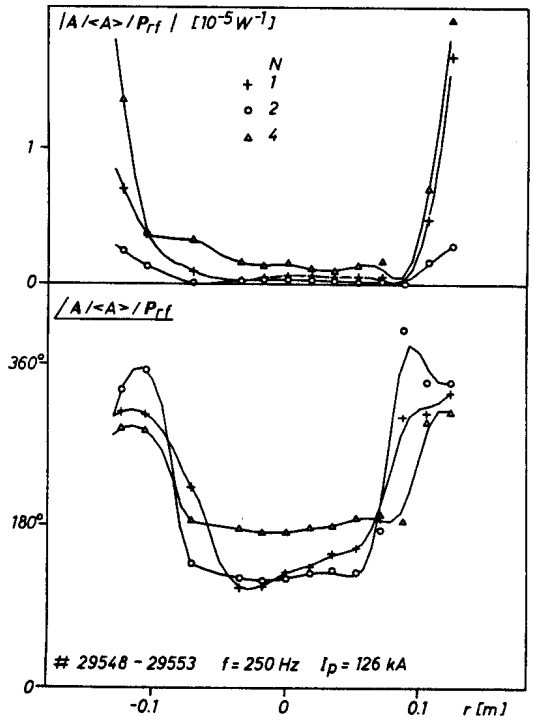

←*Fig. 5* *Profile of the Soft-X ray response for different toroidal mode numbers of excitation.*

↓*Fig. 6* *Effects of the power modulation on the sawtooth parameters.*

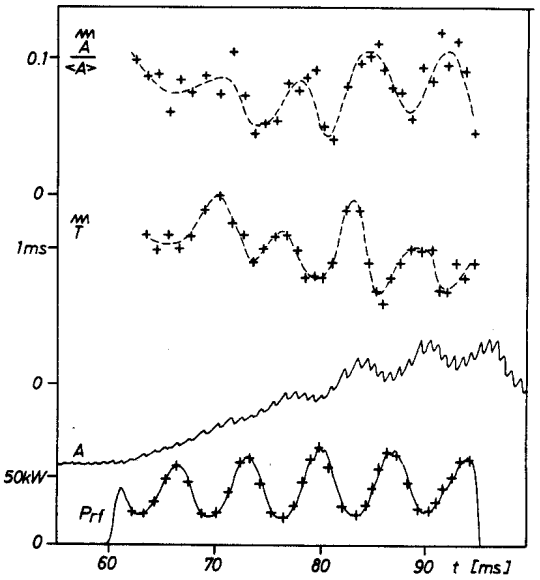

Bibliography

[1] Appert K. et al., 1987, ICPP, Kiev (invited paper), Lausanne report LRP 321/87
[2] Jahns G.L. et al., Nucl. Fus. **26**(1986)226
[3] Hartfuss H.J. et al., Nucl. Fus. **26**(1986)678
[4] Besson G. et al., 1986, 13th Europ. Conf. on Cont. Fus. and Plasma Physics, Schliersee
[5] Collins G.A. et al., Phys. Fluids **29**(1986)2260
[6] Gambier D., private communication

Acknowledgement We would like to thank Ch. Simm for his help in using the Soft-X ray diode array system. This work was partially supported by the Fonds National pour la Recherche.

DETAILED EFFECTS OF THE EXCITED WAVE SPECTRUM IN ALFVEN WAVE HEATING ON TCA TOKAMAK

B.P. Duval, A.A. Howling, B. Joye, J.B. Lister, J.-M. Moret and F. Ryter

Centre de Recherches en Physique des Plasmas
Association Euratom - Confédération Suisse
Ecole Polytechnique Fédérale de Lausanne
21, Av. des Bains, CH-1007 Lausanne / Switzerland

ABSTRACT

The launching of Alfvén Waves (AW) in the TCA Tokamak always causes a strong increase in density. Therefore the excited spectrum evolves and its effects manifest themselves on many plasma parameters. Variations in the plasma column resistance, $\beta+li/2$ and MHD activity are clearly related to the Alfvén spectrum and may indicate a modification of the current profile.

The TCA Tokamak (R,a=0.61, 0.18 m, B_ϕ = 1.5 T, $I_p \lesssim$ 130 kA) is dedicated to the study of Alfvén Wave Heating (AWH). The antenna structure comprises eight groups of poloidal antennae, four above and four below the plasma, which allows a choice of the dominant modes by changing the relative phasing of the antennae. The resonance condition for the Shear Alfvén Wave is in cylindrical geometry given by:

$$\omega^2(r) = \left(\frac{1}{R}\right)^2 \left(n + \frac{m}{q(r)}\right)^2 \left(\frac{B_\phi^2}{\mu_o \rho(r)}\right) \left(1 - \frac{\omega^2}{\omega_{ci}^2}\right)$$

where n,m are the toroidal and poloidal wavenumbers, q(r) and $\rho(r)$ are the local values of the safety factor and mass density and ω_{ci} is the

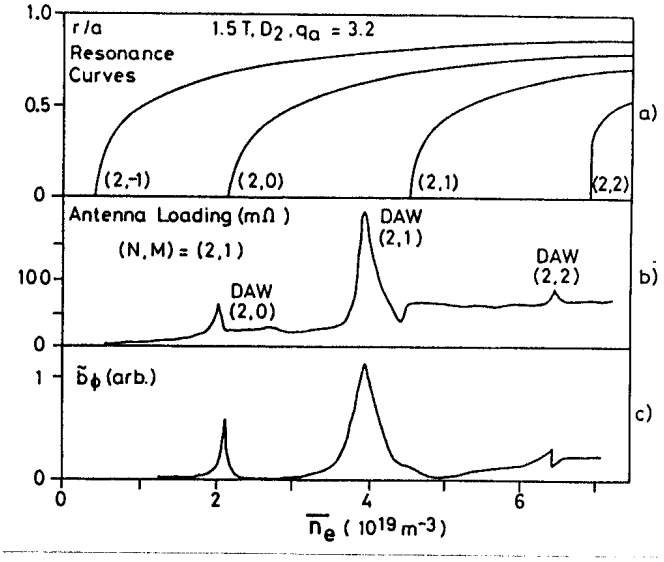

Fig. 1: Illustration of the AWH scheme

a) Radial positions of resonance surfaces

b) Antenna loading measured as a function of density

c) Amplitude of the toroidal magnetic wavefield at the rf frequency in the plasma edge

ion-cyclotron frequency. For the frequency of 2.5 MHz used for this work, the radial position of the resonance surfaces versus line-averaged density is plotted in Fig. 1a. Typical tokamak plasma profiles of T_e and n_e were assumed to calculate the radial dependance of $q(r)$ and $\rho(r)$. The Discrete Alfvén Waves (DAW) appear as peaks on the measured antenna loading (Fig. 1b) below the threshold of continua with $nq/m > 0$. The excitation is $(N,M) = (2,1)$ and the modes with $m = 0,2$ are produced by toroidal coupling.[1]

One effect of the rf power is to increase the density. The resonance surfaces then move radially outwards, as illustrated in Fig. 1. These effects complicate the interpretation of the substantial ion temperature increase. The electron temperature measured by Thomson scattering shows a strong modulation during the sawteeth[2] but only a small increase in the baseline temperature. The sawtooth slope measurements also indicate a peaked power deposition profile close to the threshold of different continua. Measurements of $(\beta+li/2)_{max}$ are plotted in Fig. 2 as a function of P_{rf} for several plasma currents. The maximum increase ($\Delta(\beta+li/2)\simeq 0.6$) occurs for the lowest plasma current. This value cannot be explained only by an increase in plasma energy since the measurement of $\Delta\beta_\perp$ gives a much smaller value (<0.2). There is therefore a significant change in the plasma internal inductance which corresponds to a significant change in the current profile.

These global measurements do not reveal the fine effects of the spectrum. The temporal evolution of some plasma parameters is shown in Fig. 3. At the beginning of the rf pulse, $\beta+li/2$ increases more rapidly than $\Delta\beta_\perp$. After the (2,1) DAW, $\beta+li/2$ decreases faster than $\Delta\beta_\perp$. This

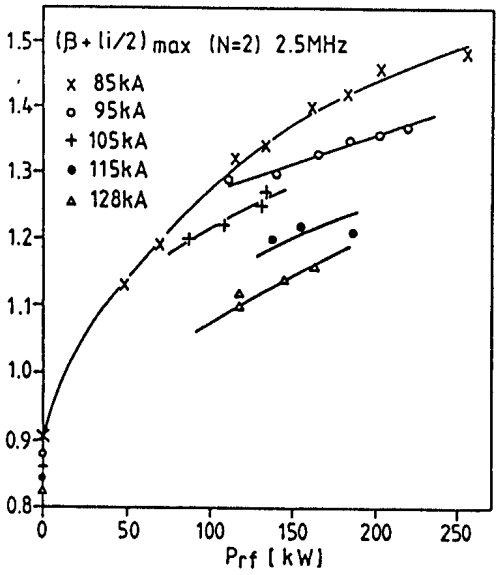

Fig. 2: Maximum value of $(\beta+li/2)$ obtained for different plasma currents

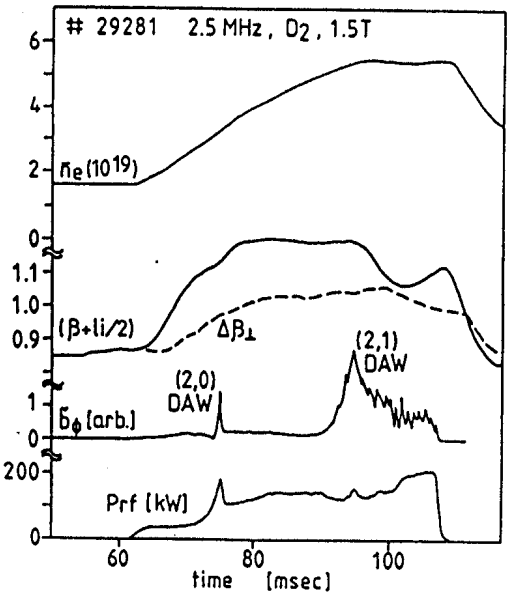

Fig. 3: Temporal evolution of $\beta+li/2$ and $\Delta\beta_\perp$ when a spectral threshold is crossed

suggests an increase in li when the rf is switched on, and a decrease after the AW thresholds. Changes in the sawtooth frequency are also provovoked by the rf power. Especially at low density, the sawteeth frequency increases sharply ($\lesssim$ 50%) near an AW threshold although the increasing density tends to decrease the frequency. Measurements of $\tau_{inc} = \Delta W/(P_{rf}+\Delta P_{oh}-\Delta \dot{W})$ also show a dependence on the spectrum. The value of 7 ms at the beginning of the pulse decreases to about 4 ms in the (2,0) continuum and drops to 1.6 ms after the (2,1) DAW. The temporal evolution of $\beta+li/2$ shows a similar drop for several different DAW modes. Figure 4 shows four conditions, namely (N,M)=(2,0) (2,1) (1,1) for

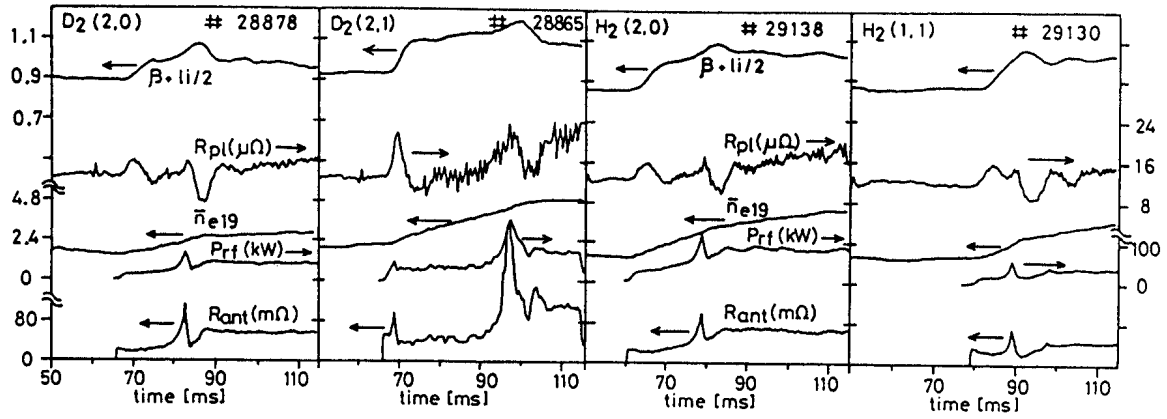

Fig. 4: Evolution of $\beta+li/2$ and R_{pl} for different excitation modes

H_2 and D_2 discharges. For all these cases, a dip in the plasma column resistance (R_{pl}) and the break in $\beta+li/2$ are associated with the arrival of a new continuum threshold. Under these different conditions, the radial positions of the next outermost surfaces are also different, meaning that the dips are clearly not identifiable with these outer surfaces. By launching a travelling wave in one or the other direction (N = +1,-1), the evolutions of $\beta+li/2$ and R_{pl} are similar apparently excluding an explanation by a direct current drive. It is also difficult to explain this fact by a strong sudden heating since the soft X-ray fluxes do not show a sudden strong increase at the centre. The most likely explanation is that the effect is inductive since the R_{pl} parameter also contains a dli/dt term. The change in power deposition profile, due to the arrival of a new resonance surface, may cause a local conductivity change. It might be expected that a change in current profile would affect the MHD stability. The MHD activity, measured as the m = even component of the Mirnov activity $|\dot{B}_\Theta(a)|$ increases or decreases with respect to the level during ohmic heating, depending on the part of the spectrum excited. We have plotted in Fig. 5 the temporal evolution of the antenna loading together with the mode activity. Just after the start of the rf pulse, the (2,-1) continuum causes a decreases in the MHD signal. The (2,0) DAW provokes a sudden rise followed by a slight decrease. Sharp peaks appear for the (2,1) and (2,2) DAWs. The evolution of these effects with rf power is illustrated in Fig. 6 where $|\dot{B}_\Theta|$ is plotted against antenna current for three different states of the excited spectrum indi-

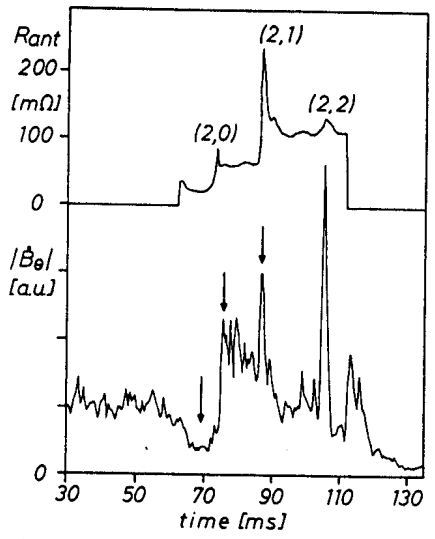

Fig. 5: Effect of the Alfvén Wave spectrum on the MHD activity (I_p = 85 kA)

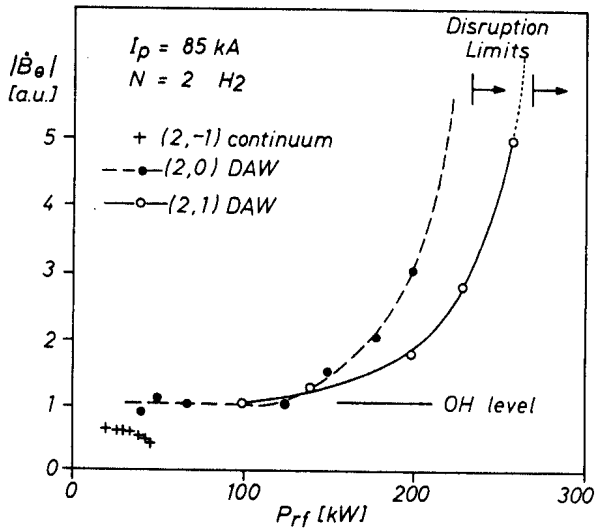

Fig. 6: MHD activity (m = even) level as a function of rf power

cated by arrows in Fig. 5. As the rf power is increased, the dramatic increase in the MHD activity at the DAWs causes the plasma to disrupt. The MHD activity is more strongly destabilised by the (2,0) DAW than by the (2,1) DAW for a given rf power. These observations are similar for the range of plasma currents studied, from I_p = 85 kA (q(a) = 4.7) to 135 kA (q(a) ~3.0).[3] At high current, however, the MHD activity decrease in the (2,-1) continuum is not measurable because the initial ohmic level is already within the noise level. The delivered rf power can be increased by over a factor of 2 between the thresholds, but this increased power level causes a bigger rise in the density leading inevitably to a disruption at the next DAW. The level of activity at which the disruptions occur is similar in ohmic and rf discharges suggesting the same self-destabilization mechanism. Possible causes of the increase in MHD are a local increase in dj(r)/dr near q=2 or an increase in the global gradient between q=1 and q=2.[4] A change in MHD activity has already been reported for ECRH.[5] The experimental evidence all points to changes in the current profile. These changes occur specifically near the mode thresholds as the structure of the excited waves alters.

Acknowledgements: This work was partly supported by the Fonds National Suisse de la Recherche Scientifique.

[1] G.A. Collins et al., Phys. Fluids 29 (1986), 2260.
[2] B. Joye et al., Phys. Rev. Lett. 56 (1986), 2481.
[3] K. Appert et al., ICPP, Kiev, April 1987 (invited paper), Lausanne Report LRP 321/87.
[4] A. Bondeson, Nucl. Fusion, 26 (1986), 929.
[5] V.V. Alikaev, K.A. Razumova, Course and Workshop on Applications of rf Waves to Tokamak Plasmas, Varenna, Vol. I (1985), 377.

STUDY OF THE BROADBAND MAGNETIC TURBULENCE IN THE TCA TOKAMAK

F. Ryter, A. Pochelon and F. Hofmann

Centre de Recherches en Physique des Plasmas
Association Euratom - Confédération Suisse
Ecole Polytechnique Fédérale de Lausanne
21, Av. des Bains, CH-1007 Lausanne / Switzerland

ABSTRACT Poloidal structures of magnetic turbulence are studied and their persistence along the magnetic lines is analysed. This can give an estimate of the minor radii of the observed turbulence.

INTRODUCTION The study of broadband magnetic turbulence features is important to determine its nature and its possible effects on the transport. This paper presents measurements of the magnetic turbulence on the TCA tokamak (B_T=1.5 T, R=61.5 cm, a=18 cm), newly equipped with 96 magnetic coils placed in the scrape-off layer. The spatial properties of the turbulence and its relation to confinement have been presented earlier[1] and this work concentrates on the study of the poloidal structure of the turbulence and its transformation along field lines. Figure 1 gives the layout of this system where the subsystems of coils A,B,E and T will be referred to as arrays. T is a vertical radial array ranging from r=20.7 cm to 27.7 cm and E is identical but in the equatorial plane. A and B are identical arrays placed symmetrically with respect to the equatorial plane and composed of 18 B_θ coils at z=±22 cm and 14 B_r coils at z=± 21.3 cm. The coils are therefore not at constant radius (20.5 cm<r<24.5 cm) but each coil is oriented to measure only either the B_r or the B_θ field component. All the B_θ coils have dimensions 10×10×5 mm^3 and all the B_r coils 10×5×5 mm^3. The small size of the coils and their close spacing allow very large poloidal mode numbers up to m ≈80 to be detected. In this study, the broadband magnetic turbulence is measured between 40 kHz and 800 kHz, well above the 10 kHz Mirnov frequency. Although the coherence is bounded between 0 and 1, due to the finite number of samples used, the coherence between two completely uncorrelated signals is 0.17.

I. RADIAL COHERENCE AND POLOIDAL MODE NUMBER The coherence between the coils of array T and E shows that the B_θ and B_r fluctuating fields are highly coherent in the radial direction between the plasma and the vacuum vessel as illustrated in Fig. 2. Thus the vacuum field model is appropriate to estimate the poloidal mode number m(B_θ) from the radial decrease of the B_θ field component. Figure 3 shows the comparison of the experimental points with this model, which yields m(B_θ)≈6 at 200 kHz and m(B_θ)≈8 at 800 kHz. This method cannot be applied to the B_r component because of the influence of the wall. We should stress that this result is obtained for a single shot in the same radial direction. Moreover, we have successfully applied this method to determine the Mirnov oscillation mode numbers m=2 and m=3, already identified independently by the standard method.

II. COHERENCE IN THE POLOIDAL PLANE The coherence between the coils in arrays A and B has been studied in detail for I_p=130 kA, q_a=3.1. No

up-down asymmetry was found and we shall not distinguish between A and B. Figures 4 and 5 show the coherence and the phase between the central B_θ or B_r coil (R=61.5 cm) and the neighbouring B_θ and B_r coils. For frequencies above 400 kHz, phase jumps of π are seen. In the B_r-B_r case of Fig. 4, they correspond to a minimum in the coherence followed by a secondary maximum as ΔR is increased. This is characteristic of a stationary wave with the statistical wavelength $\lambda_\theta(B_r)$ defined as twice the distance between two phase jumps. For frequencies below 400 kHz the phase plot is typical of a travelling wave and around 400 kHz the phase is representative of both features.

These results are also seen, although less clearly, in the B_θ-B_θ case of Fig. 5. The secondary maxima are lost, probably because the poloidal coherence length is shorter than $\lambda_\theta(B_\theta)$. We see, however, that $\lambda_\theta(B_\theta) \simeq 1.5\lambda_\theta(B_r)$. The poloidal number m can be estimated for the two cases and we find $7<m(B_\theta)<9$ for 400 kHz$<f<$800 kHz, in good agreement with the results of Fig. 3, and $9<m(B_r)<12$ for 400 kHz$<f<$800 kHz.

We also calculated the coherence between one B_r reference coil and the B_θ coils (Fig. 6). The coherence between B_r and B_θ is very low at the same position, but increases to a maximum as the separation from the reference coil is increased. The phase plot indicates that the poloidal wavelength of this structure is $\lambda_\theta(B_r)$. This figure reveals that, statistically, the turbulence in one poloidal plane is symmetrical with respect to the radial direction. The asymmetry of the curves is probably due to a small misalignment between the array and the plasma.

III. LONG DISTANCE COHERENCE The coherence in the toroidal direction has been studied between arrays T and A. Taking one B_r or B_θ coil of array T as the reference coil, the coherence with the coils of array A is measured. The resulting coherence curves are comparable with the corresponding ones given in Figs. 4, 5 and 6. The central point of the structures is displaced away from the position R=61.5 cm in such a way that the coherent structures would appear to persist along magnetic field lines. Figure 7a, for q_a=3.6, shows a good example of the results obtained for a q_a-scan. The position of the maxima depends on the frequency and the curves become broader at higher frequencies, which is opposite to the trends within one A or B array, as seen in Fig. 5. This reveals a poloidal diffusion of the coherent structures, as they propagate in the toroidal direction, stronger at higher frequencies. Moreover, as q_a is varied, the peak value of the coherence plots diminishes whereas its width increases.

From these results, we attempted to determine the radius of the magnetic surfaces on which the turbulence "propagates". For this purpose, we assume, firstly, that the poloidal structure of the turbulence is transmitted from its origin towards the arrays in the radial direction, and secondly, that the maxima of coherence in array A are the images of the reference T coil through the magnetic rotational transform. This method is shown in Fig. 7b which shows, in the poloidal plane of array A, the transformation of the radial line supporting the array T by the rotational transform of the field lines, including toroidal effects. If the coherence of the turbulence, for a given frequency, followed one field line, the position of the maximum would define the poloidal rotation of this line on its way toroidally from the position of array T to that of A

($\Delta\phi$ = 113°). We can, therefore, find the magnetic lines supporting the turbulence for each frequency, as indicated by the arrows in Fig. 7b. The higher frequencies are located at the plasma surface whereas lower frequencies are in the scrape-off layer. This method gives similar results when applied to other values of q_a between 3.1 and 8.9. Significant toroidal coherence is not restricted to that found between arrays T and A, and other measurements, not described here, show correlation over large toroidal distances (up to at least $2\pi R$).

IV. DISCUSSION We have shown, with two different methods, that modes of low poloidal numbers are involved in the magnetic turbulence and that the poloidal dispersion relation cannot be the linear extrapolation of ω/k=const., valid at low frequency (Mirnov oscillations). This would have implied m≈30 at 200 kHz and also that m increased by a factor of 4 between 200 kHz and 800 kHz. The correlation between B_r and B_θ shown in Fig. 6 implies that the B_r and B_θ fields have a common source. It is then difficult to understand how the poloidal wavelengths $\lambda_\theta(B_r)$ and $\lambda_\theta(B_\theta)$ are different by a factor of 1.5. At the present time, it is not possible to attribute this factor to experimental errors in the estimated $\lambda_\theta(B_r)$ and $\lambda_\theta(B_\theta)$, or to the physics of the turbulence. The results of paragraphs 2, 3 and 4 point to a change in the nature of the turbulence above 400 kHz. In fact, travelling waves seem to dominate the low frequency part, whereas the higher frequency part shows characteristics of stationary waves.

ACKNOWLEDGEMENTS We acknowledge the collaboration of Ch. Hollenstein, M.L. Sawley, W. Simm, discussions with P.A. Duperrex and H. Weisen and the support of the TCA Team. This work was partly supported by the Fonds National Suisse de la Recherche Scientifique.

REFERENCE [1] P.A. Duperrex et al., Phys. Lett. 106A, 133 (1984), Ch. Hollenstein et al., Cargèse Workshop 1986, Proc. edited by D. Grésillon, M.A. Dubois, or Lausanne report LRP 306/86, Sept. 1986.

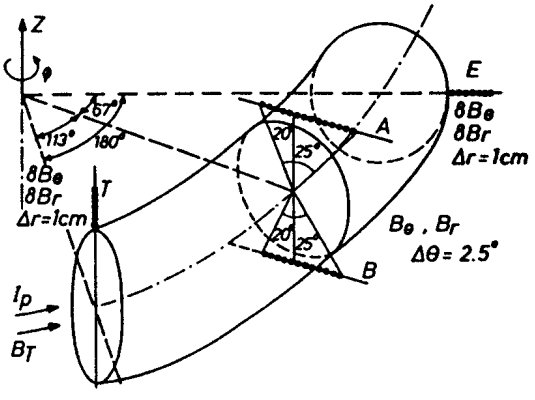

Fig. 1: Layout of magnetic probes

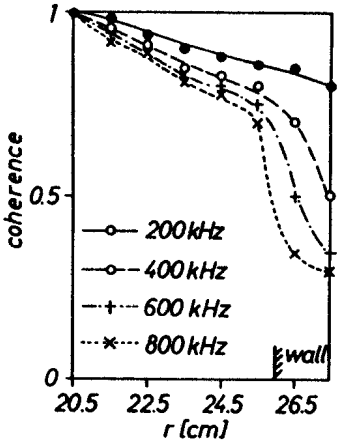

Fig. 2: Radial B_θ-B_θ coherence: coherence and phase between the coil at r=20.5cm and the others.

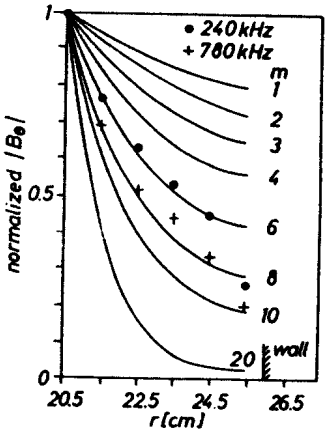

Fig. 3: Radial decrease of the fluctuating B_θ amplitude; solid lines: calculated points: measured

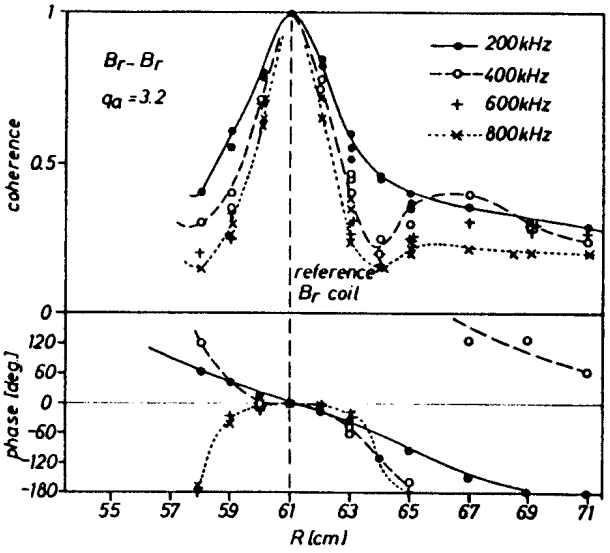

Fig. 4: Poloidal B_r-B_r coherence in array A: coherence and phase between the central coil at R = 61 cm and the others

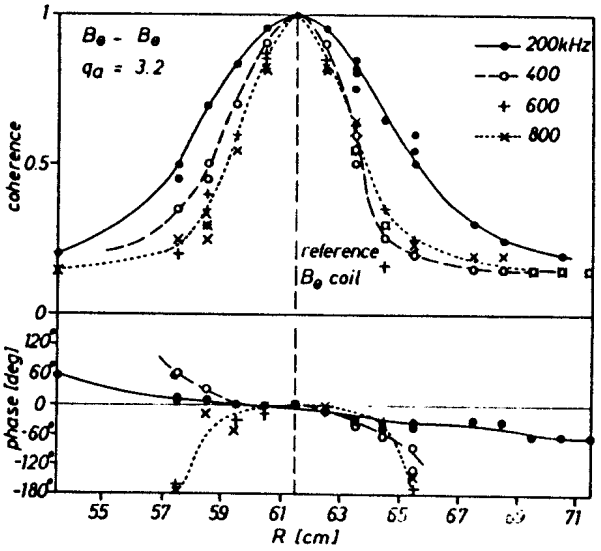

Fig. 5: Poloidal B_θ-B_θ coherence in array A: coherence and phase between the central coil at R=61.5cm and the others

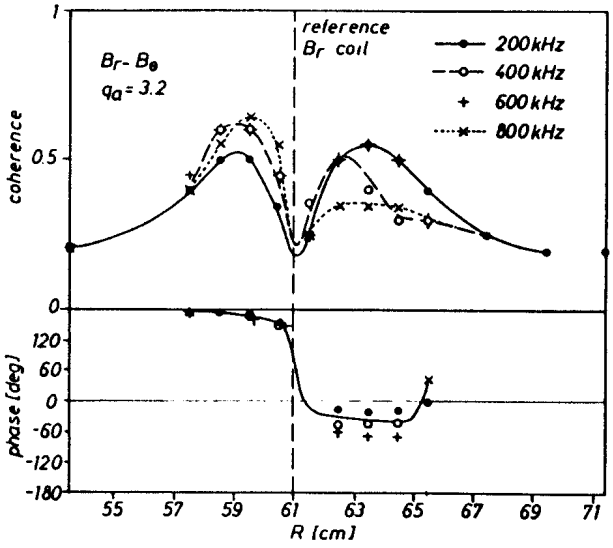

Fig. 6: Poloidal B_r-B_θ coherence in array A: coherence and phase between the central B_r coil and the B_θ coils

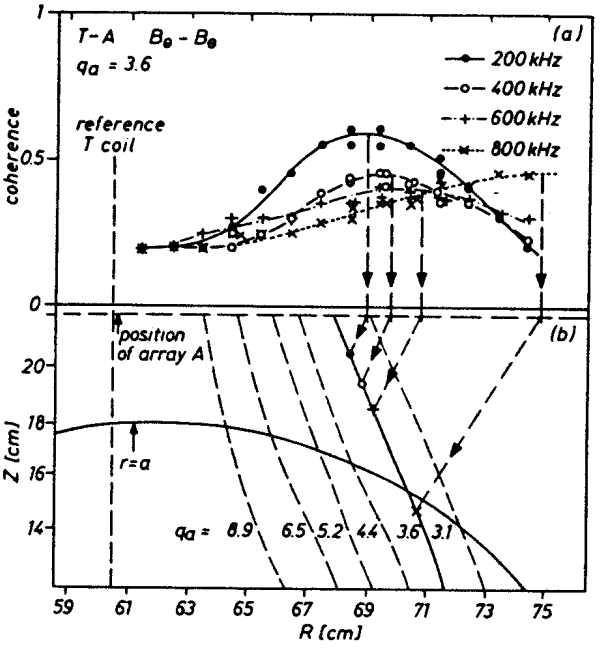

Fig. 7: (a) Poloidal B_θ-B_θ coherence between reference T coil and A coils (b) Image, in the poloidal plane of array A, of the radius supporting array T, through the rotational transform for different q_a values. The arrows, along the radial directions indicate how the position of the coherence maxima is related to the magnetic lines.

TURBULENT DENSITY FLUCUTATIONS IN THE TCA TOKAMAK

H. Weisen, R. Behn and Ch. Hollenstein

Centre de Recherches en Physique des Plasmas
Association Euratom - Confédération Suisse
Ecole Polytechnique Fédérale de Lausanne
21, Av. des Bains, CH-1007 Lausanne / Switzerland

I. INTRODUCTION

This paper summarizes the results of our investigation on the spectral characteristics, spatial structure and scaling with plasma parameters of low frequency density fluctuations in ohmically heated TCA plasmas (B_ϕ=1.5T, R=61cm, a=18cm, $I_p \leq 170$kA, $\bar{n}_e \lesssim 10^{14}$cm^{-3}, $T_e(0) \simeq$ 800eV) using the phase contrast method[1,2]. This imaging method is suitable for the investigation of fluctuations in a wide band of wave numbers, $0.5 \leq k_\perp \leq 20$rad/cm for the measurements presented. It uses a 23×4cm wide CO_2 laser beam transmitted through the plasma and produces an image where the small phase shifts ($\phi \lesssim 10^{-3}$ radians) due to refractive perturbations are revealed as corresponding intensity variations which are detected by liquid nitrogen cooled HgCdTe detectors. In the wave number range of interest the device is equivalent to a fast high resolution interferometer with high sensitivity ($\sim 10^{-5}$ radians for Δf=1MHz).

The two detectors, D1 and D2 in Fig. 1, can be positioned at will in the image $\sum'$ of the outer two thirds of plasma midplane $\sum$. As the depth of field exceeds by far the dimensions of the plasma, the measurements are line integrated and free of scintillation effects[3,1].

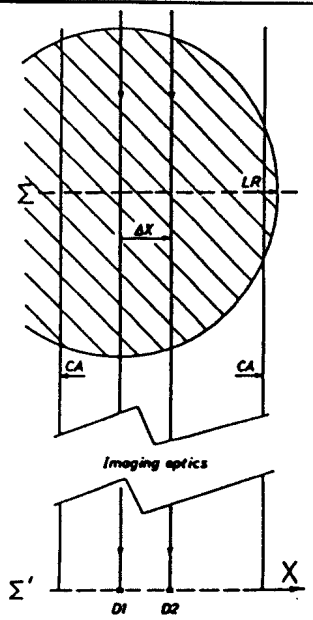

Fig. 1 Setup and accessibility

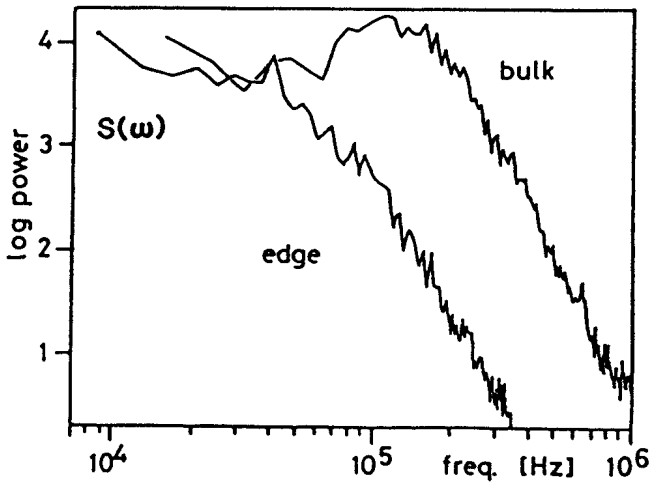

Fig. 2 Frequency spectra

II. SPECTRAL CHARACTERISTICS

The frequency spectra depend on the position x of the viewing chord (Fig. 2). For positions close to the plasma center ($x/a \lesssim 1/2$) the spectra are higher in frequency by a factor of 2 to 3 than those obtained for chords close to the edge. The latter are in fact very similar to the density fluctuation spectra obtained by Langmuir probes in the scrape-off layer[4]. Figure 3 shows the normalized cross spectrum $P_{12}(f)=\langle I_1^*(f) I_2(f)\rangle (\langle I_1^* I_1\rangle\langle I_2^* I_2\rangle)^{-1/2}$ of the signals from the two detectors as a function of detector separation. For these measurements detector D1 was fixed at x=0 while D2 was scanned during a series of reproducible discharges with $\bar{n}_e=2.5\cdot10^{13}$ cm^{-3}, $q(a)\simeq3.3$. (Only the real part of P_{12} is shown, the imaginary part being about an order of magnitude smaller.) Spatial Fourier transformation of these data yields a conditional spectrum s(k f) and subsequent multiplication by the frequency spectrum s(f) gives the power spectrum s(k,f) shown in Fig. 4. A clear dispersion with an average velocity of 5×10^5cm/s is observed. This is consistent with the drift velocity defined by $v_p=c\nabla p/eB_\phi n_e$ and a factor of 3 higher than the diamagnetic drift velocity $v_D=cT_e/eB_\phi L_n$. Summing over frequencies yields the wave number spectrum of Fig. 5, with a maximum at $k_\theta\simeq1.3$ rad/cm corresponding to $k_\theta r_s=0.25$ if $\langle T_e\rangle=400$eV is assumed ($r_s=c_s/\omega_{ci}$).

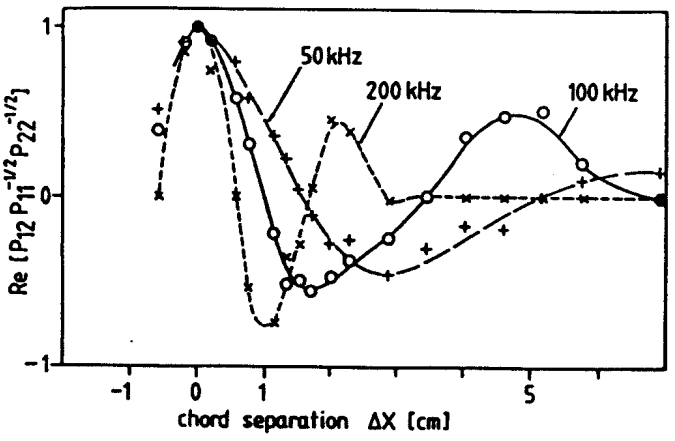

Fig. 3 (left) Cross power as a function of detector separation

Fig.4 (bottom left) Power spectrum $s(k_\theta,f)$ Contour line spacing is a factor of 1.4

Fig. 5 (below) Wavenumber spectrum $s(k_\theta)$

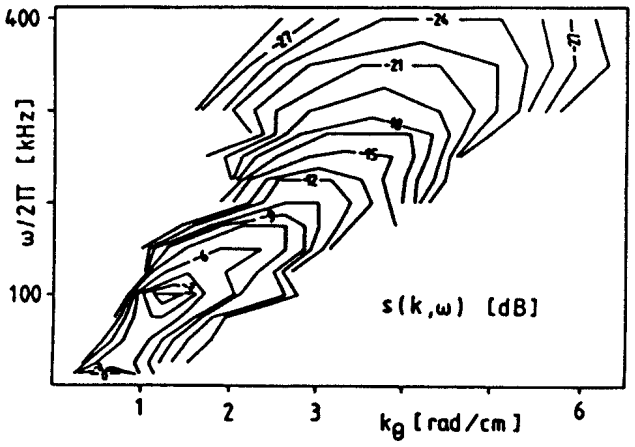

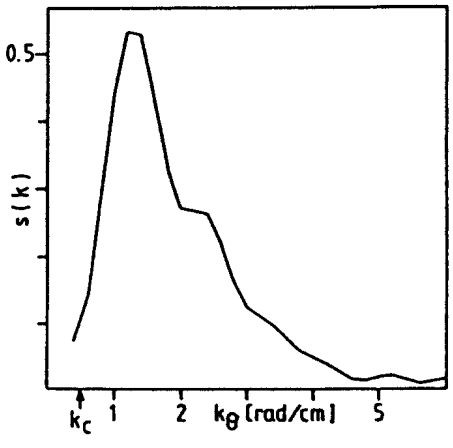

III. SPATIAL DISTRIBUTION AND AMPLITUDE OF TURBULENCE

The spatial profiles of line integrated rms fluctuation levels are shown in Fig. 5 for two characteristic frequency bands, centered at 50 and 200kHz ($\Delta f/f_0=0.31$). The continuous lines are for $\bar{n}_e=2.5\times10^{13}cm^{-3}$, the broken ones for $\bar{n}_e=4.5\times10^{13}cm^{-3}$. (Levels are normalized to $\bar{n}_e$.) For f<100kHz the amplitude peaks near the edge, whereas for f>140kHz it peaks in the plasma interior at x/a≈1/3 on the low field side. The amplitude on the low field side at x/a=0.25 is about twice the amplitude at x/a=-0.25, indicating the importance of toroidal effects. A similar asymmetry had already been observed on TEXT[6].

From these line integrated profiles we expect radial profiles that show a similar behaviour, with low frequencies dominant at the edge and the higher frequencies in the interior. The correlation measurements also yield higher phase velocities in the interior ($v_{ph}\approx4$ to 5×10^5cm/s for x/a<1/2) than near the edge where $v_{ph}\approx2\times10^5$cm/s. The local fluctuation $\tilde{n}_{rms}$ levels can be estimated from the line integrated level $\tilde{N}_{rms}$ by the relation $\tilde{N}_{rms}\approx\tilde{n}_{rms}\times\sqrt{L\times l}$, where L is the size of the turbulent region (L≈a) and l is the correlation integral scale, which was obtained from the correlation measurements[1]. Estimates for x/a=1/2 and 3/4 yield relative fluctuations levels $\tilde{n}_{rms}/n_e$ of 2.5% and 5 to 7% rms. Probe measurements in the scrape-off layer show fluctuation levels of 20 to 40% rms. The absolute levels are consistent with Kadomtsev's mixing length estimate[7] $\tilde{n}_e/n_e\approx(\langle k_\perp\rangle L_n)^{-1}$, as $\langle k_\perp\rangle\approx2$rad/cm for all three cases and $L_n\approx18$, 7 and 2cm for x/a=1/2, 3/4 and 1.1 respectively.

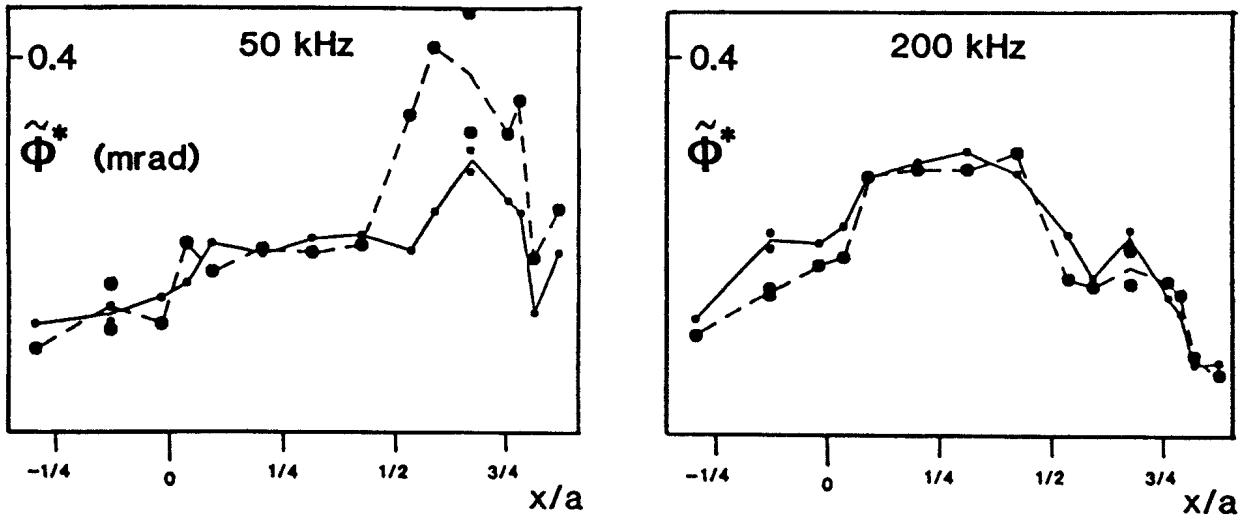

Fig. 6 Level of fluctuation as a function of detector position for f=50 and 200 kHz expressed as rms phase shift $\tilde{\phi}$ of the probe beam normalized to $\bar{n}_e$: $\tilde{\phi}^* = \tilde{\phi}\cdot(2.9\cdot10^{13}cm^{-3}/\bar{n}_e)$.

The scaling of $\tilde{N}_{rms}$ with plasma parameters also follows the mixing length rule, $\tilde{N}_{rms}/\bar{n}_e$ being roughly constant throughout the operational domain of TCA, with no systematic dependence on the plasma current I_p[4,1].

IV. DISCUSSION

Although the fluctuations observed appear to have the general features of drift wave turbulence, the possibility of an identification with any particular mode or existing theoretical model is very uncertain. Whether the fluctuations are electrostatic or electromagnetic remains an open question. The observed phase velocities, which exceed the estimated drift velocity v_D by a factor of three, can be interpreted either as a result of plasma rotation, or as an indication of electromagnetic fluctuations such as tearing or rippling modes. Also it is not possible to decide whether the low values of $k_\perp r_s$ observed is a result of inverse cascading[8] from the most unstable domain ($k_\perp r_s \sim 1$) of electrostatic drift waves or simply correspond to the most unstable region of e.g. rippling modes in toroidal geometry[9].

Quasilinear estimates of the heat flux for the level of fluctuations observed, assuming they are electrostatic, are comparable in magnitude to the ohmic power in TCA[1]. If they are to account for the anomalous losses, however one has to admit that the phase relation between $\tilde{E}$ and $\tilde{n}_e$ varies as a function of plasma parameters; to our knowledge this phase relation is not yet accessible to experimental investigation.

To conclude we note that, although an extensive characterisation of the density fluctuations was obtained, important questions about their nature and their relevance to confinement remain unanswered. Further progress will depend on the possibility of measuring fluctuations of magnetic field and temperature and the phase relation between fluctuating quantities.

Acknowledgements - This work has been partially supported by the Fonds National Suisse de la Recherche Scientifique. Thanks are extended to J.B. Lister, W.C. Simm and A. Pochelon.

References

[1] H. Weisen, Thesis No. 659, EPF - Lausanne (1986).
[2] H. Weisen, Infrared Phys. 25, (1985), 543.
[3] L.E. Sharp, Plasma Phys. 25, (1983).
[4] Ch. Hollenstein et al., ECA 10C, I p. 144, Schliersee 1986.
[5] H. Weisen et al., Plasma Phys. and Contr. Fusion 28, (1986), 1161.
[6] D.L. Brower et al., Phys. Rev. Lett. 54, (1986) 689.
[7] B.B. Kadomstev, "Plasma Turbulence", Academic press, 1965.
[8] M. Watakani and A. Hasegawa, Phys. Fluids 27, (1984), 611.
[9] A. Rogister, Plasma Phys. and Contr. Fusion 28 (1986), 547.